International Journal of Control Theory and Applications

ISSN : 0974-5572

Volume 10 • Number 36 • 2017

A Charge Based Compact Physical Model with Unified 2DEG for AlGaN/AlN/GaN MISHEMTs including SCEs

S. Baskaran[a] A. Mohanbabu[b] and N. Mohankumar[c]

[a]*Department of ECE, S.K.P Engineering College, Tiruvannamalai, India*

E-mail: skpbaskar@gmail.com

[b]*Research Scholar, Anna university, India*

E-mail: babumohan95@gmail.com

[c]*Department of ECE, SKP Engineering College, Tiruvannamalai, India*

E-mail: nmkskpec@gmail.com

Abstract: In this paper, we have derived the physics-based analytical expressions for 2DEG (ns) and Fermi level (Ef) as an explicit function of thermal biases valid for all regions of operations scalable with physical parameters are developed which includes the two lowest subbands (E0 and E1) in the triangular well. With this unified Ef model, charge based drain current expressions for Metal Insulated Semiconductor (MIS) HEMT is derived. The compact drain current model is validated with experimental data of MISHEMT for all regions show a good agreement in I-V characteristics of the device. The effect of SCEs on the model is included and discussed and the role of different capacitances as a function of bias voltage is explored in detail. Moreover, the proposed device is analyzed for high-frequency applications by using TCAD simulations. The model is tunable and hence applicable to a wide range of HEMT and MISHEMT devices of different geometries and construction.

Keywords: *AlGaN/AlN/GaN, capacitance model, High-K AlN, Metal Insulated High Electron Mobility Transistor (MISHEMT) with two subbands.*

1. INTRODUCTION

AlGaN/GaN heterostructure based High Electron Mobility Transistors (HEMTs) exhibit various advantages such as high electron mobility, high saturation drain current, low switch on-resistance and large off-state breakdown voltage [1]. These unique properties make them a promising candidate for high-frequency, high speed and high power applications [1]. The wide band gap and high breakdown voltage of AlGaN/GaN materials limit the performance and reliability of a device operation in high temperature environments [2]. Inspite of these, MISHEMTs (Metal Insulated High Electron Mobility Transistors) have attracted a lot of attention due to much reduced gate leakage and better restrain of current collapse [3]. The major concern in HEMTs is the current collapse effect, which degrades the DC and RF parameters under large input signals. Hence the performance

of AlGaN/GaN HEMTs for high power and high temperature applications can be improved by using insulating gate dielectrics which reduces the gate leakage current, enhances the operating voltage and shields the device surface [4, 5]. In these, nitride-based dielectrics especially AlN is most preferred due to the larger band gap and smaller lattice mismatch [6,7]. $Al_xGa_{1-x}N$/AlN/GaN MISHEMTs with a spacer layer has unique features such as high two-dimensional electron gas (2DEG) sheet carrier density (n_s) and carrier mobility owing to their excellent DC and RF performance [8]. Therefore the wide band gap of AlN Spacer layer reduces the two-dimensional electron gas (2DEG) and electron-wave penetration into the AlGaN barrier layer that significantly increases the sheet charge density (n_s) and mobility with reduced scattering effects [10,11]. Moreover they alleviate poor thermal stability and reduce the power consumption owing to simpler circuit design.

A compact model (CM) physically describes the behavior of a generic HEMT device in all operating regions making it suitable for the circuit design. Recently, there has been a lot of literature in HEMT and MISHEMT CMs [2]–[11]. Those models are complex and rely on a large number of fitting parameters. Most of the existing HEMT models depend on an accurate description of the 2DEG at the heterostructure junction. Due to the various energy levels and Fermi potential positions that need to be considered while calculating the charge in the region, the charge and current models often end up being complex and unattractive for circuit design [5]. In this analysis, analytical expressions for n_s with two subbands (E_0 and E_1) in the triangular well with respect to the conduction band edge at the heterointerface is considered in the model formulation. The model formulation and their description are given in Table 1.

The schematic representation of the proposed $Al_xGa_{1-x}N$/AlN/GaN MISHEMT is shown in Fig.1 and the corresponding band diagram of MISHEMT including the first two subbands are shown in Fig.2 in which physical parameters are shown by the respective labels. The layer sequence from top to bottom is Gate/Insulator/AlGaN barrier/AlN spacer/GaN channel, with a two dimensional electron gas (2DEG) channel formed at the interface between the Un-intentionally doped (UID) AlN spacer and GaN channel.

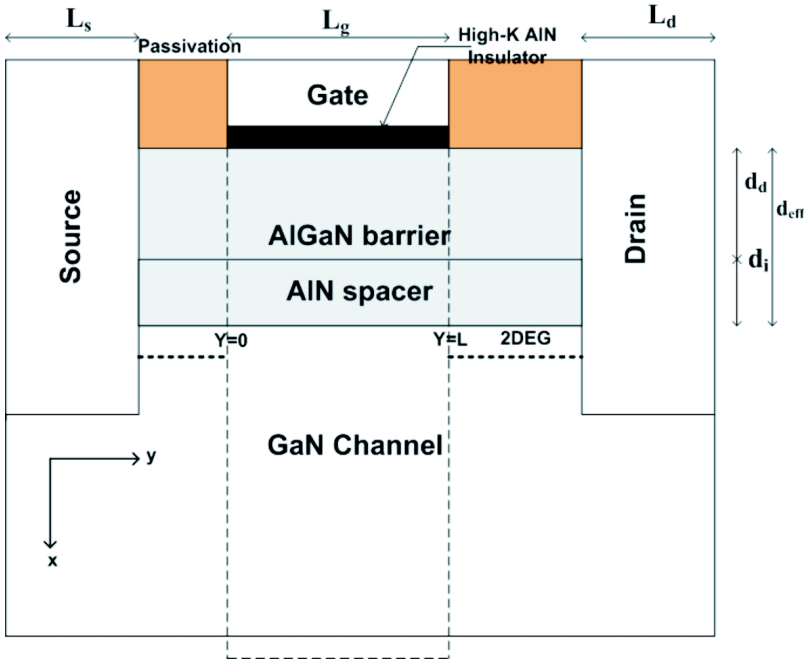

Figure 1: Schematic cross-section of $Al_xGa_{1-x}N$ /AlN/GaN MIS-HEMT

The Fermi potential (in volts), E_f, is referenced to the conduction-band edge at the heterointerface ($x = 0$). Electrostatic potential (E) and voltage (V) (in volts) with reference to the Fermi level of the body are shown in the energy band diagram (Fig 2).

In this paper, a unified drain current (I_{ds}) model with respect to gate to source voltage (V_{gs}) including the first two subbands E_0 and E_1 are analyzed. Also the unified single piece explicit (E_f) solution, along with the simple gate charge (Q_G) model is formulated and expressions for gate to source capacitance (C_{gs}) and gate to drain capacitance (C_{gd}) models are derived. The compact drain current model is validated with experimental data of MISHEMTs for all regions (Subthreshold to strong inversion) including short-channel effects SCEs (Channel length modulation (CLM), Velocity saturation) which shows a good agreement. The paper is organized as follows: Model structure and formulation in Section 1, polarization and threshold voltage model are presented in Section 2. Also the sheet carrier density and expressions for E_f are analyzed in Section 2.1. Section 3 describes the drain current model and Section 3.1, 3.2, 3.3 describe the short-channel effects SCEs on the drain current model. Section 4 discusses the charge and capacitance models. Section 5 discusses the validated results of the model with experimental data. The conclusions are arrived in Section 6.

1.1. Model structure and Formulation

We consider only two subbands, the sheet carrier density n_s in the interface can be calculated using the Fermi–Dirac distribution as follows [18]

$$n_s = D_w \int_{E_0}^{E_1} \frac{dE}{1+e^{\left(q\left(E-E_f\right)/kT\right)}} + D_w \int_{E_1}^{\infty} \frac{dE}{1+e^{\left(q\left(E-E_f\right)/kT\right)}}$$

where, $D_w = qm^*/\pi h^2$ and $1+e^{\left(q\left(E-E_f\right)/kT\right)}$ represent the Fermi–Dirac probability function which is continuous from the base of the quantum well to infinity with $V_{th} = kT/q$. Evaluating the equation (1) by using integral $[\int dx/(1+e^x) = -\ln(1+e^{-x})]$ yields

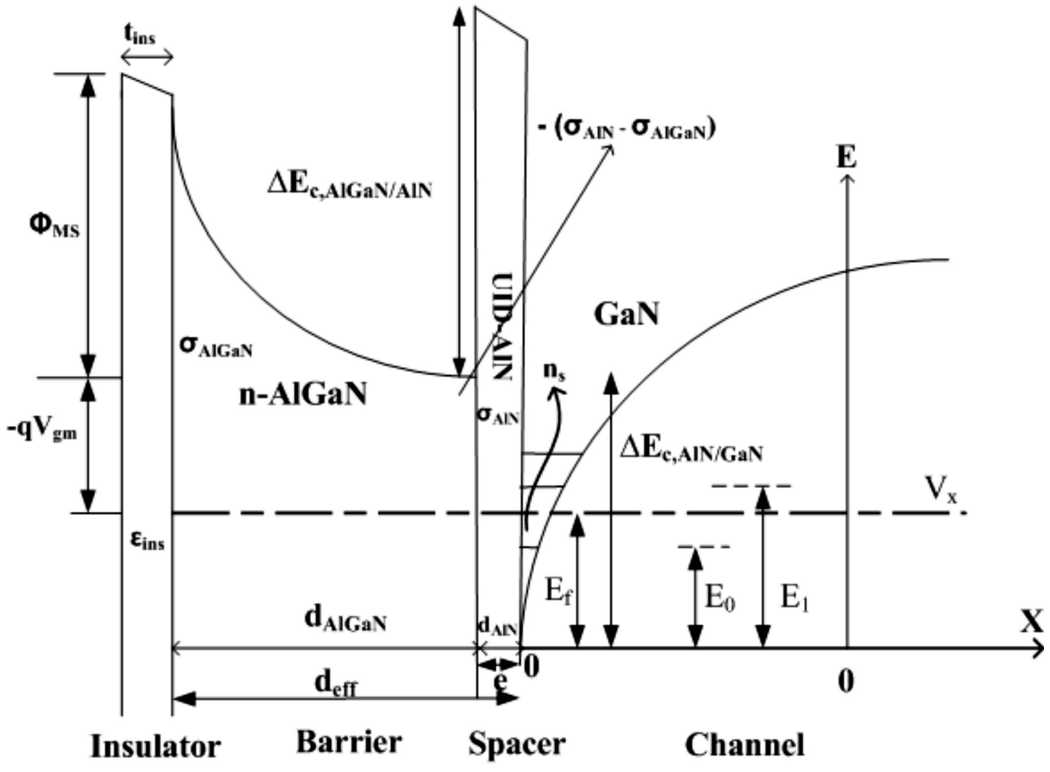

Figure 2: Energy-band diagram of a $Al_xGa_{1-x}N$/ Unintentionally doped (UID) AlN/GaN heterostructure MISHEMT

$$n_s = D_w \times KT \ln\left[1 + e^{\left(E_f - E_0\right)/kT}\right] + D_w \times KT \ln\left[1 + e^{\left(E_f - E_1\right)/kT}\right] \tag{1}$$

At low temperature the above equation reduces to,

$$n_{s,0} = D_w \left(E_f - E_0\right),$$

if only the first band is occupied (1a)

$$n_{s,1} = D_w \left\{\left(E_f - E_0\right) + D_w \left(E_f - E_1\right)\right\},$$

if two subbands are occupied. (1b)

The analytical expression of n_s with two subbands in the quantum well is given as [1]

$$n_s = D_w v_{th} \ln\left[\left(1 + e^{(E_f - E_0)/v_{th}}\right)\left(1 + e^{(E_f - E_1)/v_{th}}\right)\right] \tag{2a}$$

$$E_0 = \gamma_0 n_s^{2/3} \tag{2b}$$

$$E_1 = \gamma_1 n_s^{2/3} \tag{2c}$$

where E_f is the Fermi level of the bottom of the triangular quantum well. $\{\gamma_0, \gamma_1, D\}$ are experimentally determined parameters is shown in Table 1.

Following the analysis in [1], n_s in (2*a*) is related to the gate (V_{gs}) and channel (V_x) voltages by neglecting the variation of Fermi level through Gauss' law as

$$n_s = \frac{C_d}{q}(V_{gm} - E_f - V_x) \tag{3}$$

$$n_s = \frac{\varepsilon_{eff}}{q d_{eff}}(V_{gm} - E_f - V_x) \tag{3a}$$

where V_{gm} is gate overdrive voltage, $C_d = \varepsilon_{eff} / d_{eff}$ is the depletion capacitance and V_x is channel potential along from source to drain. Raising both sides of the equation (3) to the 2/3 power we get,

$$n_s^{\frac{2}{3}} = \left(\frac{C_d}{q}\right)^{2/3} \left(V_{gm} - E_f\right)^{2/3} \tag{4}$$

Using Taylor series expansions and expanding right hand term we get,

$$= \left(\frac{C_d}{q}\right)^{\frac{2}{3}} \left[V_{gm}^{\frac{2}{3}} - \frac{2}{3} V_{gm}^{\frac{2}{3}} \frac{E_f}{V_{gm}} + \frac{1}{6} V_{gm}^{-\frac{4}{3}} {E_f}^2\right] \tag{5}$$

For compact modeling purposes, we have restricted the series to order k = 2.

$$n_s^{\frac{2}{3}} \approx \left(\frac{C_d}{q}\right)^{2/3} V_{gm}^{2/3} \left[1 - \frac{2}{3}\frac{E_f}{V_{gm}}\right] \tag{6}$$

Applying this observation and using the approximation $\ln(1 + e^x) = x$ for $x >> 1$ to (2*a*), the solution for n_s and E_f can be written as

$$\frac{n_s}{D_w V_{th}} = \frac{E_f - E_o}{V_{th}} + \frac{E_f - E_1}{V_{th}} \tag{7}$$

Simplifying (7) we get the equation for n_s and E_f,

$$n_s = 2D_w E_f - D_w \left\{\gamma_0 n_s^{2/3} + \gamma_1 n_s^{2/3}\right\} \tag{8}$$

$$E_f \approx n_s \frac{V_{th}}{2} + \frac{(\gamma_0 + \gamma_1)}{2} n_s^{2/3} \tag{9}$$

The expressions of gate overdrive voltage V_{gm} can be extracted from (3) to establish a correlation between V_{gm} and n_s given as

$$V_{gm} = \frac{n_s q d_{eff}}{\varepsilon e_{ff}} + E_f \tag{10}$$

In addition, (10) can be extended to any channel point and substituting the expression of E_f from (9) by considering V as the local quasi-Fermi potential.

$$V_{gm} - V = \frac{n_s q d e_{ff}}{\varepsilon e_{ff}} + n_s \frac{V_{th}}{2} + \frac{(\gamma_0 + \gamma_1)}{2} n_s^{2/3} \tag{11}$$

Therefore, we have dV with respect to the charge density dn_s obtained from the derivative of (11), which enables integration over the charge density, it can be given as

$$-\frac{dV}{dn_s} = \frac{qd}{\varepsilon} + \frac{V_{th}}{2} + \frac{(\gamma_0 + \gamma_1)}{3} n_s^{-1/3} \tag{12}$$

$$dV = -\left[\frac{qd}{\varepsilon} + \frac{V_{th}}{2} + \frac{(\gamma_0 + \gamma_1)}{3} n_s^{-1/3} \right] dn_s \tag{13}$$

The gradient in total polarization at the AlGaN/AlN/GaN interface should cause a polarization induced interface sheet density. The concentration of polarization charge of each interface σ derived from the tensor of the wurtzite crystals is derived from the following:

$$\begin{cases} \sigma_{Al_xGa_{1-x}N/\,AlN} = (P_{SP}^{AlN} - P_{SP}^{AlN}) - (-P_{SP}^{Al_xGa_{1-x}N} + P_{Pz}^{Al_xGa_{1-x}N}) \\ \sigma_{AlN/GaN} = (P_{SP}^{GaN} + P_{Pz}^{GaN}) - (P_{SP}^{AlN} - P_{SP}^{AlN}) \\ \sigma_{\text{int}} = \sigma_{Al_xGa_{1-x}N/\,AlN/GaN} = \sigma_{GaN} - \sigma_{AlN} - \sigma_{Al_xGa_{1-x}N} \\ = (P_{SP}^{GaN} + P_{Pz}^{GaN}) - (P_{SP}^{AlN} - P_{SP}^{AlN}) - (P_{SP}^{Al_xGa_{1-x}N} + P_{Pz}^{Al_xGa_{1-x}N}) \end{cases} \tag{14}$$

The total induced net polarization density σ_{int} which forms at the hetero interface is the difference of the polarization in the barrier $Al_xGa_{1-x}N$, the spacer σ_{AlN} and the polarization in the GaN σ_{GaN}, these total polarization charges abruptly, causing a fixed two-dimensional polarization charge density at the interface. The mole fraction-dependent parameters used here are defined in Table I. By assuming the barrier layer being fully depleted, the polarization dependent threshold voltage V_{off} and effective capacitance C_d (per unit area) between the gate and 2DEG of the Metal insulated HEMTs can be obtained as [1]

$$V_{off} = \phi_{MS} - \Delta E_{c,eff} - \left(\frac{t_{ins}}{\varepsilon_{ins}} \right) q N_D \left(d_{eff} - e \right) \tag{15}$$

$$-\frac{qN_D}{2\varepsilon_{eff}} \left(d_{eff} - e \right)^2 - \frac{q\sigma_{\text{int}} d_{eff}}{\varepsilon_{eff}}$$

where N_d is the doping concentration of the barrier layer, ε_{eff} and ε_{ins} are the permittivity of the barrier layer and insulator, respectively, φ_{ms} is the work difference between metal and intrinsic semiconductor and σ_{int} is the polarization induced charge density at the heterointerface.

2. SHEET CARRIER DENSITY MODEL

2.1. Subthreshold Region $E_f > E_0$ and $E_f > E_1$

In the subthreshold (off) region, $E_f >> E_0$ and E_1 and therefore $E_f - E_o$ and $E_f - E_1 \approx E_f$ [4]. Applying this observation and using the basic approximation $\ln(1+e^x) \approx e^x$ for x>>1 to (2a), and invoking (3), the solution for n_s can be written in terms of a Lambert's function W as

$$n_{s,sub} = 2D_w V_{th} W e^{\frac{V_{gm}}{V_{th}}} \tag{17}$$

The subthreshold regional E_f solution is found by substituting the expression of E_f from equation (3) to be a Lambert's function W as

$$\frac{C_d}{q}(V_{gm} - E_f - V_x) = 2D_w V_{th} W\left\{e^{\frac{V_{gm}}{V_{th}}}\right\} \tag{18}$$

$$E_f = V_{gm} - \frac{2qD_w V_{th}}{C_d} W\left\{e^{\frac{V_{gm}}{V_{th}}}\right\} \tag{19}$$

Weak Inversion Region $E_0 < E_f < E_1$:

For $E_0 < E_f < E_1$, In this region, the electrons are localized to the quantum well. Equation (2a) can be approximated When using the condition $\ln(1+e^x) \approx e^x$ as

$$n_{s,\mathrm{moderate}} = D_w V_{th}\, e^{(E_F - E_0)/V_{th}} \approx D_w V_{th}\, e^{(E_F - \gamma_0 n_s^{2/3})/V_{th}} \tag{20}$$

Substituting the expression for $n_s^{2/3}$ from (5) in (6), the $n_{s,\mathrm{moderate}}$ can be approximated by

$$n_{s,\mathrm{moderate}} = D_w V_{th} e^{\frac{\left[E_f(1+\eta) - \frac{3}{2}V_{gm}\eta\right]}{V_{th}}} \tag{21}$$

we take $$\eta = \left(\frac{2\gamma_0}{3V_{gm}}\right)\left[\frac{C_d}{q}V_{gm}\right]^{\frac{2}{3}}$$

Hence, (3) can still be used to simplify (21). Substituting (3) into (21), can be expressed as

$$\frac{C_d}{q}(V_{gm} - E_{f,\mathrm{mod}}) = D_w V_{th} e^{\frac{\left[E_f(1+\eta) - \frac{3}{2}V_{gm}\eta\right]}{V_{th}}} \tag{22}$$

$$E_{f,\mathrm{moderate}} = V_{gm} - \frac{V_{th}}{C_d} \cdot e^{\frac{-3\eta V_{gm}}{2V_{th}}} \cdot e^{\frac{(1+\eta)E_f}{V_{th}}} \tag{23}$$

By inspection, (23) has a solution for E_f in the form of a Lambert function, W, if η is treated as a parameter and $\vartheta = \frac{-3\eta}{2} + (1+\eta)$

$$E_{f,\mathrm{moderate}} \cong V_{gm} - \frac{V_{th}}{1+\eta} W\left[\frac{(1+\eta)e^{\vartheta\left(\frac{V_{gm}}{V_{th}}\right)}}{C_d}\right] \tag{24}$$

Strong Inversion Region $E_1 < E_f$:

When E_f goes above E_1, electrons no longer remain localized in the quantum well. They start to spill out occupying other regions, thus leading to the formation of parallel channels. The sheet charge density $n_{s,0}$ and $n_{s,1}$ due to subbands E_0 and E_1 from (2*a*) & (2*b*) are given as

$$n_{s,0} = D_w E_f - D_w \gamma_0 n_s^{3/2} \tag{25}$$

$$n_{s,1} = 2D_w E_f - D_w(\gamma_0 + \gamma_1) n_s^{3/2} \tag{26}$$

Thus, from (6), the $(n_s)^{2/3}$ term can be substituted into (25) and (26), we obtain (27) and (28). In the strong-inversion region, if $E_0 < E_f < E_1$, from (2*a*)-(2b) using $\ln(1 + e^x) \approx x$, n_s can be approximated as

$$n_{s,0} = D_w E_f - D_w \gamma_0 \left(\frac{C_d}{q}\right)^{2/3} \left[V_{gm}^{2/3} - \frac{2}{3} V_{gm}^{2/3} \frac{E_{f,0}}{V_{gm}}\right] \tag{27}$$

Likewise, if $E_f > E_1$, n_s can be approximated as

$$n_{s,1} = 2D_w E_f - D_w(\gamma_0 + \gamma_1) \left[V_{gm}^{2/3} - \frac{2}{3} V_{gm}^{2/3} \frac{E_{f,1}}{V_{gm}}\right] \tag{28}$$

Combining (3) with (2*a*) and (2*b*), explicit regional E_f solutions can be derived as [1]

$$\begin{aligned} E_{f,0} &= x * V_{gm} \\ E_{f,1} &= y * V_{gm} \end{aligned} \tag{29}$$

$$x = \frac{C_d / qD_w \, V_{gm}^{1/3} + \gamma_0 \left(C_d / q\right)^{2/3}}{(1 + C_d / qD_w) V_{gm}^{1/3} + \frac{2\gamma_0}{3} \left(C_d / q\right)^{2/3}}$$

$$y = \frac{C_d / 2qD_w \, V_{gm}^{1/3} + \left(\frac{\gamma_0 + \gamma_1}{2}\right) \left(C_d / q\right)^{2/3}}{(1 + C_d / 2qD_w) V_{gm}^{1/3} + \left(\frac{\gamma_0 + \gamma_1}{3}\right) \left(C_d / q\right)^{2/3}}$$

A unified E_f model for the strong-inversion region can be constructed by the following smoothing function:

$$E_{f,strong} = V_{gm} \theta_{eff}$$

$$\theta_{eff}(x(V_{gm,eff}), y(V_{gm,eff}), \alpha) = 0.5\left(x + y + \alpha - \sqrt{(x - y - \alpha)^2 - 4\alpha x}\right) \tag{30}$$

$V_{gm,eff}$ is introduced [15] to prevent any incalculable results. It goes to zero when $V_{gs} - V_{off}$ is negative. For positive $V_{gs} - V_{off}$, $V_{gm,eff}$ approaches $V_{gs} - V_{off}$. δ_s is a smoothing parameter.

$$V_{gm,eff} = 0.5\left(V_{gs} - V_{off} + \sqrt{(V_{gs} - V_{off})^2 + 4\delta_s}\right) \tag{31}$$

To get a unified E_f model, the three regional solutions are joined together using appropriate smoothing functions [1].

$$E_{f,\,\text{unified}} = \text{Vgm} - \Delta E_f$$

$$\Delta E_f = \frac{2V_{th}(1 - \theta_{eff}) \ln(1 + e^{\frac{V_{gm}}{V_{th}}})}{1 + C_d(1 - \theta_{eff}) e^{\frac{-V_{gm}}{V_{th}}}} \tag{32}$$

However, to improve accuracy, we propose to use a unified form that combines the two regional models. Here, we have used an approximate unified explicit expression that covers all the operating regions from deep subthreshold to full active gate bias to obtain the charge carrier concentrations at the source and drain. From this ,we proposed a model for n_s and we can write

$$n_{s,unified} = \frac{C_d}{q}\left\{\frac{2V_{th}(1-\theta_{eff})\ln(1+e^{\frac{V_{gm}}{V_{th}}})}{1+C_d(1-\theta_{eff})e^{\frac{-V_{gm}}{V_{th}}}}\right\} \tag{33}$$

3. DRAIN CURRENT MODEL

To develop a compact DC model for the devices, we use the typical physics based potential-based form expression under the drift diffusion framework and including the velocity saturation effect can be obtained as follows as

$$I_{ds} = \mu_{eff} C_d \frac{W}{L_g}\left(V_{gs} - V_{off} - \overline{V_{ds,eff}} + 2V_{th}\right)\times V_{ds,eff} \tag{34}$$

where W and L_g are the gate width and length of the device with $V_{gm,s/d} = V_{gs} - V_{off} - \Delta E_f(V_c)$, $V_c = V_{s/d}$, $\overline{V_{ds,eff}} = (V_{gm,s} - V_{gm,d})/2$ represent the potential at the source and drain ends, respectively and δ is a fitting parameter,. Here, μ_{eff} and μ_0 is the effective mobility and low field mobility at room temperature T and is given by

$$\mu_{eff} = \frac{\mu_0}{\sqrt{1-\delta\left(\frac{V_d - V_s}{E_T L_g}\right)^2}}.$$

As the operating power of GaN MISHEMT device increases, it has become important to include effects like velocity saturation) into this core drain current model which is explained and shown below.

3.1. Velocity saturation

With an increase in the longitudinal electric field E, the carrier gain sufficient energy eventually causes saturation of the carrier velocity. When velocity saturation takes place, the saturation voltage is modeled using the approach commonly used in many MOSFET models that has been applied for MISHEMTs by treating the 2DEG as an inversion charge sheet on a body. Velocity saturation may occur at the drain or source end depending on the terminal voltage V_d and $V_{s,}$ given by the effective drain-source voltage at the source and drain end is given by [15]

$$V_{ds,eff} = V_{d,eff} - V_{s,eff} = \left\{\begin{matrix} V_{s,eff} = \upsilon\{V_s, V_{s,sat}\} \\ V_{d,eff} = \upsilon\{V_d, V_{d,sat}\} \end{matrix}\right\} \tag{35}$$

The saturation field is given by

$$E_{sat,x} = 2V_{sat}/\mu_{0,x} \quad (x = s,d) \tag{36}$$

$$\begin{cases} V_{d,sat} = \dfrac{V_{go}(V_s)L_g E_{sat,s}}{V_{go}(V_s) + L_g E_{sat,s} + 4V_{th}} + V_s \\ V_{s,sat} = \dfrac{V_{go}(V_d)L_g E_{sat,d}}{V_{go}(V_d) + L_g E_{sat,d} + 4V_{th}} + V_d \end{cases} \tag{40}$$

where V_{sat} is the saturation velocity, μ_0 is the Low-field mobility and the effective mobility μ_{eff} are extracted from a given core drain model. These effective drain-source voltages give a smooth transition between the applied drain-source voltages.

3.2. Channel length modulation (CLM)

In the saturation region, the channel current tends to saturate with an increase in drain source voltage across the drain end with y = L

$$I_{ds,sat} = I_{ds}(1+\lambda V_{ds,eff}) \tag{37}$$

where λ is the channel length modulation parameter [8] and is given in table 1. So the drain currents with channel length modulation effects are considered.

3.3. Transconductance g_m

For the optimization of advanced FETs in high frequency applications, the g_m plays a significant role. The g_m specifies the current carrying capability of the device for analyzing microwave performance. By variation of I_{ds} with respect to V_{gs} is defined by [8]

$$g_m = \left.\frac{dI_{ds}}{dV_{gs}}\right| V_{ds} = \text{constant} \tag{38}$$

4. GATE CHARGE AND CAPACITANCE MODEL

The gate charge can be obtained by integrating the charge density along the channel over the gate area and drain current along the channel is given as [16]

$$Q_g = W\int_0^{L_g} qn_s(V_g, V_x)dx \tag{39}$$

Thus the drain-source current with considering the energy relaxation of channel electrons I_{ds} can be simply discussed using the following expression [17]

$$I_{ds} = w\mu qn_s\frac{dv}{dx} = \frac{w}{L}\int_{Vs}^{Vd} qn_s\mu dv \tag{40}$$

With dx term in (39) can be substituted with (40) which will change the integration variable from x to V.

$$Q_g = \frac{W^2q^2\mu}{I_{ds}}\int_{V_s}^{V_d} n_s^2 dv \tag{41}$$

Therefore, we get the expression for charge per unit area and it can be written as

$$Q_g = WL_g q\frac{\int_{V_s}^{V_d} n_s^2 dV}{\int_{V_s}^{V_d} n_s dV}$$

$$= WLq\frac{\frac{q}{3C_d}(n_{drain}^3 - n_{source}^3) + \frac{(\gamma_0+\gamma_1)}{8}(n_{drain}^{8/3} - n_{source}^{8/3}) + \frac{V_{th}}{4}(n_{drain}^2 - n_{source}^2)}{\frac{q}{2C_d}(n_{drain}^2 - n_{source}^2) + \frac{(\gamma_0+\gamma_1)}{5}(n_{drain}^{5/3} - n_{source}^{5/3}) + \frac{V_{th}}{2}(n_{drain} - n_{source})} \tag{42}$$

The above specified model for gate charge Q_g is used to obtain a model for capacitance with two subbands to predict device behavior at high frequency power switching analysis. The gate-source and gate-drain capacitances can now be calculated using the partial differentiations of the gate charge with respect to the corresponding source and drain terminal voltages. Therefore, the capacitances are obtained as

$$C_{Gx} = WLq\frac{\frac{\partial f(n)}{\partial V_x}g(n) - f(n)\frac{\partial g(n)}{\partial V_x}}{(g(n))^2} \tag{43}$$

The two integrals at the numerator and denominator in (41) can be represented as $f(n)$ and $g(n)$, respectively, and integrating after changing the integration variable using (42) gives

$$\begin{aligned} f(n) &= f_{diff}(n_{drain}) - f_{diff}(n_{source}) \\ &= \frac{q}{3C_d}(n_{drain}^3 - n_{source}^3) + \frac{(\gamma_0+\gamma_1)}{8}(n_{drain}^{8/3} - n_{source}^{8/3}) + \frac{V_{th}}{4}(n_{drain}^2 - n_{source}^2) \\ g(n) &= g_{diff}(n_{drain}) - g_{diff}(n_{source}) \\ &= \frac{q}{2C_d}(n_{drain}^2 - n_{source}^2) + \frac{(\gamma_0+\gamma_1)}{5}(n_{drain}^{5/3} - n_{source}^{5/3}) + \frac{V_{th}}{2}(n_{drain} - n_{source}) \end{aligned} \tag{44}$$

$$\begin{cases} f_{diff}(n_x) = \frac{q}{3C_d}(n_x^3) + \frac{(\gamma_0+\gamma_1)}{8}(n_x^{8/3}) + \frac{V_{th}}{4}(n_x^2) \\ g_{diff}(n_x) = \frac{q}{2C_d}(n_x^2) + \frac{(\gamma_0+\gamma_1)}{5}(n_x^{5/3}) + \frac{V_{th}}{2}(n_x) \end{cases} \tag{45}$$

where f_{diff} and g_{diff} are assigned numerator and denominator variable for gate charge Q , $n_x = n_{source}$, $V_x = V_s$ with $C_{Gx} = C_{GS}$ at the source terminal and $n_x = n_{drain}$, $V_x = V_d$ with $C_{Gx} = C_{GD}$ at the drain terminal. From (42) to (44) the derivatives of $f_{diff}(n_x)$ and $g_{diff}(n_x)$ can be written as

$$\frac{\partial f(n)}{\partial V_x} = \frac{\partial f_{diff}(n_x)}{\partial V_x}, \frac{\partial g(n)}{\partial V_x} = \frac{\partial g_{diff}(n_x)}{\partial V_x} \tag{46}$$

Finally, the formula to find the capacitance (i.e., gate-to-source and gate-to-drain capacitance) can be computed using the equation below

$$\begin{cases} \frac{\partial f_{diff}(n_{source/drain})}{\partial V_{source/drain}} = \left\{\frac{qn^2_{source/drain}}{C_d} + \frac{(\gamma_0+\gamma_1)}{3}(n^{5/3}_{source/drain}) + \frac{V_{th}}{2}n_{source/drain}\right\}\frac{dn_{source/drain}}{dV} \\ \frac{\partial g_{diff}(n_{source/drain})}{\partial V_{source/drain}} = \left\{\frac{qn_{source/drain}}{C_d} + \frac{(\gamma_0+\gamma_1)}{3}(n^{2/3}_{source/drain}) + \frac{V_{th}}{2}\right\}\frac{dn_{source/drain}}{dV} \end{cases} \tag{47}$$

With

$$dn_{source/drain} = \frac{dV_{source/drain}}{\left(\frac{q}{C_g}\right) + \frac{(\gamma_0+\gamma_1)}{3}n^{-1/3}_{source/drain} + \frac{V_{th}}{2}}$$

From (47), We can see that the partial derivative of f(n) and g(n) are equivalent to derivative of $f_{diff}(n_x)$ and $g_{diff}(n_x)$ at the respective terminal given by equations (47). Therefore, the gate-source and the gate-drain capacitances can now be expressed as

$$C_{GS/GD} = WL_g q\frac{\frac{\partial f_{diff}(n_{source/drain})}{\partial V_{source/drain}}g(n) - f(n)\frac{\partial g_{diff}(n_{source/drain})}{\partial V_{source/drain}}}{(g(n))^2} \tag{48}$$

The above proposed modeled equations is for capacitance with two-subbands which improves the accuracy of the model.

4.1. Cutoff frequency (f_t)

The unity gain cutoff frequency (f_t) is a figure of merit for analyzing MIS-HEMT performance at microwave frequencies. The cutoff frequency is calculated using g_m, C_{gs} and C_{gd} and the relationship [8] can be obtained as

$$f_t = \frac{g_m}{2\pi(C_{gs} + C_{gd})} \tag{49}$$

5. RESULTS AND DISCUSSION

To explore the performance enhancements of MISHEMT and to prove the validity of the proposed model, the results are compared with conventional MISHEMT structures and experimental data, respectively. By the derived model of the sheet charge density, terminal charges, and all I–V and C–V characteristics of a GaN MISHEMT device can be predicted and analyzed with respect to different geometrical parameters and bias conditions with the inclusion of subband E_1 improves the accuracy in sub threshold and moderate inversion region compared to saturation region.

The 2DEG charge density is analyzed and compared against numerical solution for experimental data [3] at T=300K for $Al_{0.25}Ga_{0.75}N$/AlN/GaN-MISHEMT for gate length L_g=2.5µm & width W=60µm. In Fig 3, we plot the dependence of 2DEG sheet charge density (n_s) on gate to source voltage (V_{gs}). The curve is divided into three regions. In the sub threshold region, the 2DEG density shows exponential relationship with V_{gs} and when the device is ON, it exhibits a linear relationship for further increasing the $V_{gs.}$ The free carriers in the AlGaN layer screens the gate to source bias V_{gs} and thereby 2DEG density becomes saturated. From the graph, it is clear that the presence of the AlN layer increases the conduction band discontinuity between AlGaN barrier and GaN channel, thus the piezoelectric polarization effect was enhanced and the 2DEG density is increased owing to of alloy disorder scattering reduction due to the suppression of carrier penetration from the GaN channel into the AlGaN layer [8].

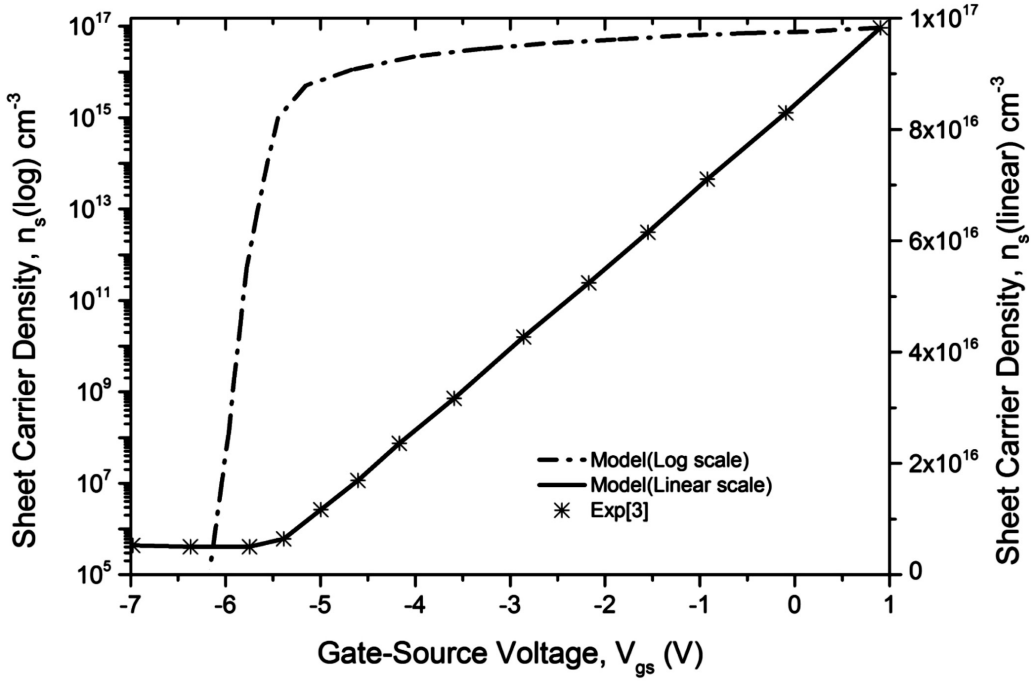

Figure 3: Comparison of modeled sheet carrier density n_s with experimental data [3] for $Al_{0.25}Ga_{0.75}N$/AlN/ GaNMISHEMT. Data plot n_s in both logarithm and linear scale is verified with experimental data [3]

Fig.4a shows the output I_{ds}-V_{ds} characteristics of $Al_{0.25}Ga_{0.75}N$/AlN/GaN MISHEMT with L_g = 2.5µm & W = 60µm for various V_{gs}. The obtained result value shows a good agreement with compared experimental data [3]. Fig.4b shows the comparison of the I_{ds}-V_{ds} of $Al_{0.3}Ga_{0.7}N$/AlN/GaN MISHEMT with L_g = 0.5µm & W = 50µm for V_{gs}. A device with a much shorter gate length, 0.5 µm, was also modeled. The Self heating effects (SHEs) were observed at higher drain voltage values. The consideration of these short channel effects in the model enabled the reproduction of the device behavior for the full operating range of voltages.

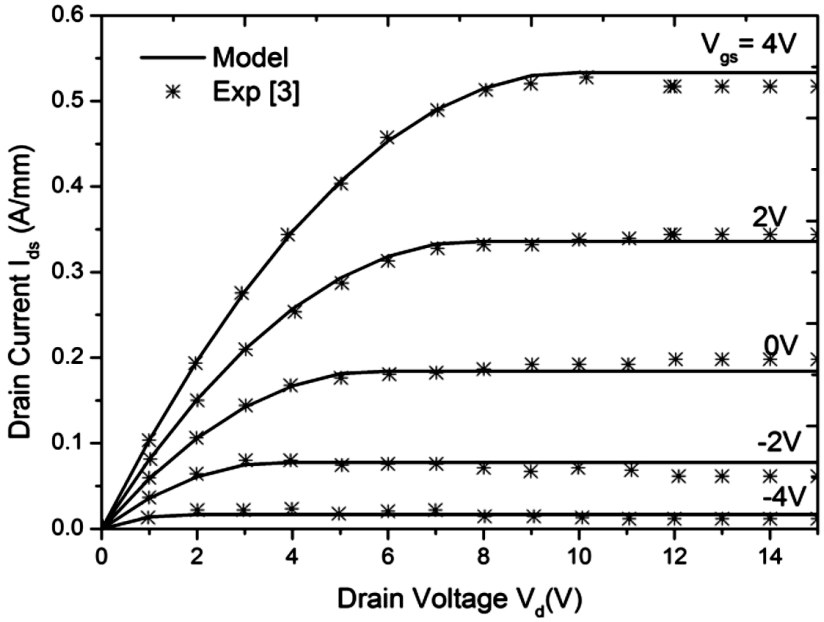

Figure 4: (*a*) Comparison of modeled I_{ds}-V_{ds} characteristics with experimental data for $Al_{0.25}Ga_{0.75}N$/GaN with AlN MISHEMT for gate length and width L_g = 2.5µm & W = 60µm Experimental data is taken from [3]

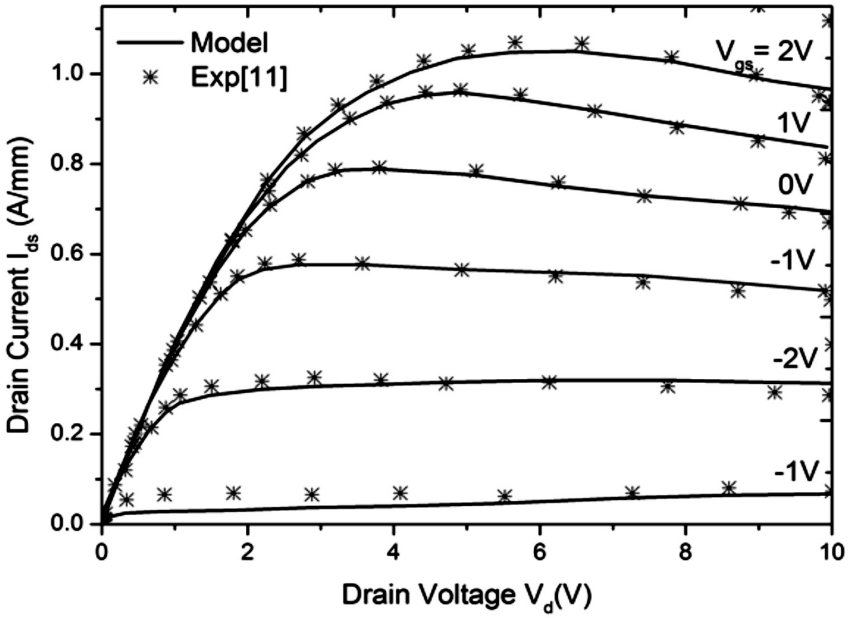

Figure 4: (*b*) Comparison of modeled I_{ds}-V_{ds} characteristics with experimental data for $Al_{0.3}Ga_{0.7}N$/GaN with AlN-MISHEMT gate length and width L_g = 0.5µm, W = 50µm .Experimental data is taken from [11].

From the Fig 4a & b, it is evident that the drain current I_{ds} increases rapidly with gate to source voltage V_{gs}, this is due to fact that, the carriers move faster than anticipated because of velocity saturation. MISHEMTs yield higher drain current as well as a higher transconductance than those of the HEMTs. This can be explained by the higher effective velocity of the GaN channel electrons and reduced series resistance in these devices with insulating gate layers [13]. A decrease in I_{ds} with increasing V_d is due to the presence of SCEs.

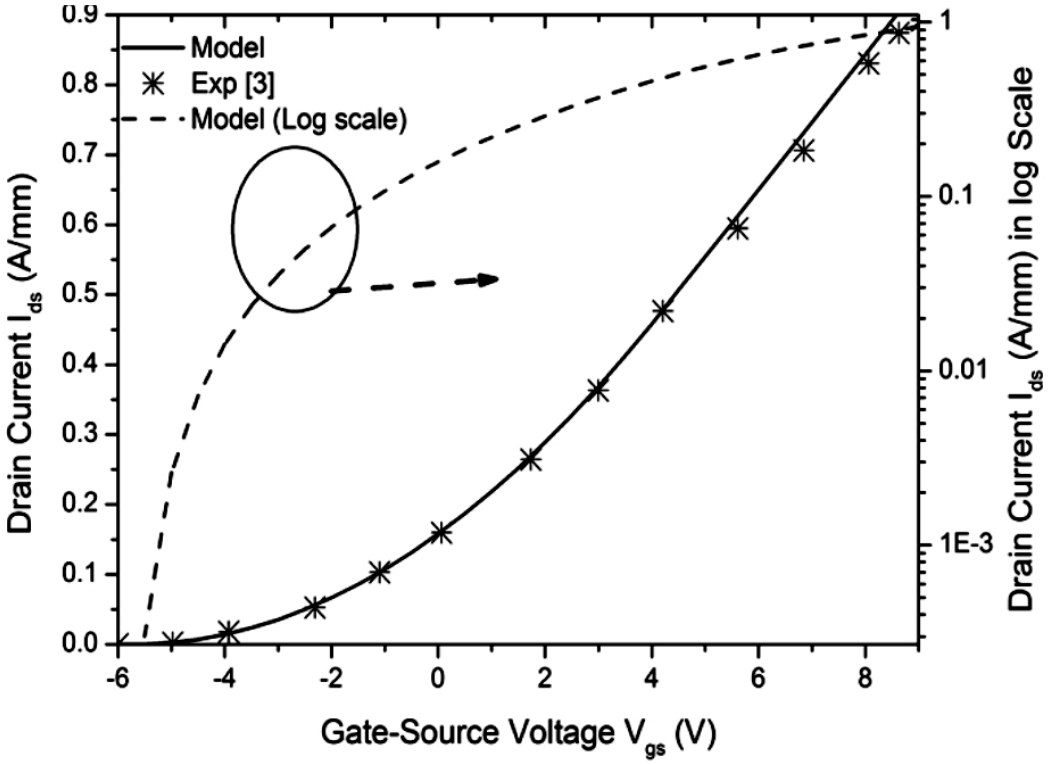

Figure 5: (*a*) Comparison of modeled I_{ds}-V_{gs} characteristics with experimental data for $Al_{0.25}Ga_{0.75}N$/GaN with AlN-MISHEMT for gate length and width L_g =2.5µm, W=60µm. Experimental data is taken from [3].

The presence of AlN dielectric suppresses the gate leakage and increases the drain current (I_{ds}) due to its high dielectric constant. From the graph, it clearly shows that increased gate length and decreased gate width will lead to decreased drain current. In both cases we observe a good agreement between the model and the experiment give excellent fit in the subthreshold region also. Fig 5a shows the I_{ds}-V_{gs} device transfer characteristics of $Al_{0.25}Ga_{0.75}N$/AlN/GaN MISHEMT compared with experimental data [3] for gate length L_g = 2.5µm and width W = 60µm with a drain voltage of 15V. The transconductance (g_m) shows the current carrying capability of device and it can be measured by varying the gate voltage (V_{gs}) for different values with constant drain voltage (V_d). The typical g_m is a function of the gate voltage of the devices, investigated is shown in Fig. 6a & 6b which is compared with experimental data [3,11]. Fig.6a shows the variation of g_m with respect to gate voltage (V_{gs}) of $Al_{0.25}Ga_{0.25}N$/AlN/GaN MISHEMT with a drain voltage of 15 V. Although the MISHEMT have lower g_m in comparison to HEMT, they have almost constant variation of transconductance for a wide range of gate source voltages, which makes it useful for high performance amplifications. Fig.6b shows the comparison of modeled g_m with experimental data [11] of $Al_{0.3}Ga_{0.7}N$/AlN/GaN MISHEMT with a drain voltage of 5V. The obtained modeled g_m value is 289 mS/mm showing good agreement with the experimental data [11]. It is clear that the g_m obtains its maximum value at very less gate voltage (V_{gs}) attributing to current collapse due to trapped charges in the source side and this effect is nullified by the AlN insulating layer by decreasing gate leakage mechanism owing to higher drain current (I_{ds}) [11].

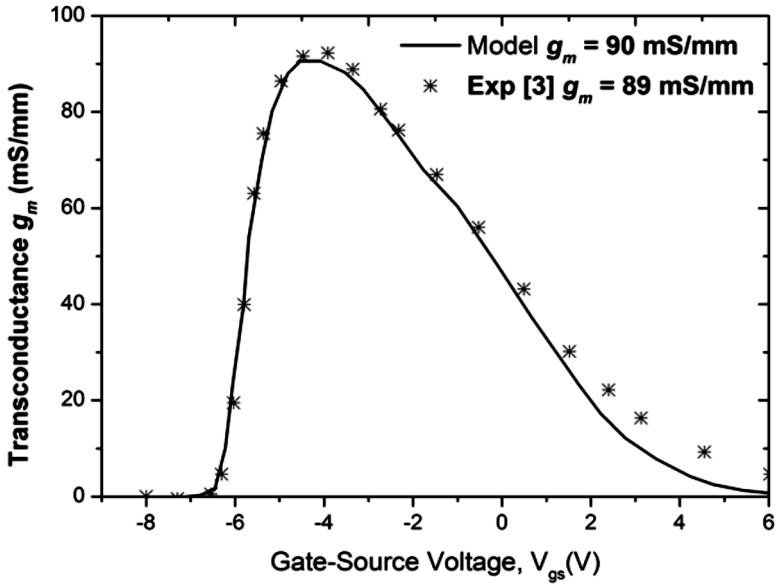

Figure 6: (*a*) Comparison of modeled g_m characteristics with experimental data for $Al_{0.25}Ga_{0.75}N$/GaN with AlN-MISHEMT for gate length and width L_g = 2.5µm & W = 60µm Experimental data is taken from [3]

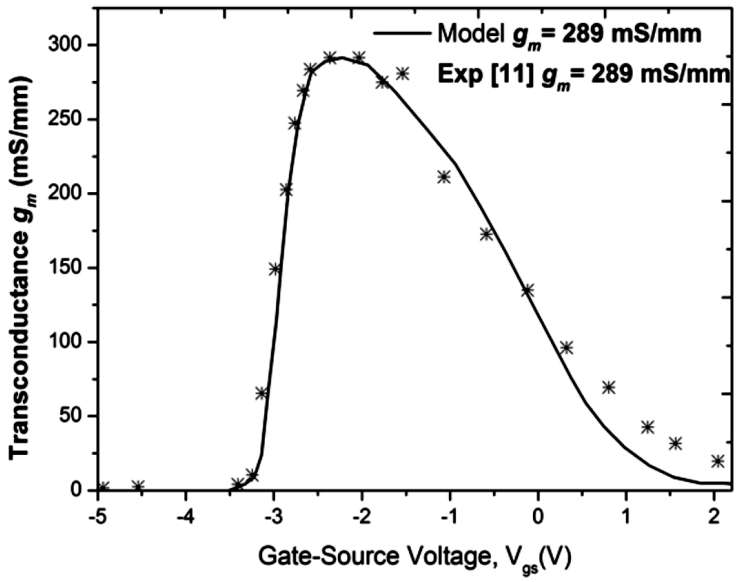

Figure 6: (*b*) Comparison of modeled g_m characteristics with experimental data for $Al_{0.3}Ga_{0.7}N$/GaN with AlN-MISHEMT gate length and width L_g=0.5µm & W=50µm . Experimental data is taken from [11].

Fig 7a,7b & 7c shows the variation of C_{gs} with V_{gs} for different Al mole fractions and different dimensions of MISHEMTs are compared with experimental data [3,11,12]. From the Fig 7a, 7b & 7c, shows that the effect of C_{gs} on the drain bias is weak, when the device is OFF. As the 2DEG sheet density is primarily monitored by gate voltage (V_{gs}), hence owing to low 2DEG density in the channel, the gate to source fringing capacitance is low. As the device is turned ON, C_{gs} increases rapidly as the gate accumulates the positive charges until the parasitic channel in AlGaN layer begin to screen the gate voltage and thereafter C_{gs} starts decreasing slightly due to increased gate controllability [16]. The slight decrease in the C_{gs} measured over the saturation region indicates an additional parasitic capacitance contribution associated with the AlGaN layer.

Fig.8 shows a plot for gate-drain capacitance C_{gd} versus V_d for a V_{gs} of 1V. From the graph, we find that there is a steady decrease in gate-drain capacitance C_{gd} as the drain bias increases, resulting from a gradual loss of drain control over the channel charge. The modeled C_{gd} = 3.45 pf/mm shows fine agreement with the experimental data [3] which validates charge modeling. Sheet carrier concentration to energy level (i.e.; Interface carrier concentration n_s) depends heavily on subband energies E_0 and E_1 in the potential well at the heterointerface in the triangular well using well known equation $E_{0/1} = \gamma_{0,1} n_s^{2/3}$. So, consideration of two lowest subbands create accuracy in predicting the amount of charge (ie; electrons) transferred across the interface [16,17].

Fig.9 shows the variation of cutoff frequency f_t with respect to gate to source voltage at the drain voltage of V_d=15 V. f_t is one of the major RF performance metric that validates the device performance at higher frequencies. From this Fig 9, it is clear that owing to increased transconductance and decreased the parasitic fringe capacitance leads to improvement in overall f_t of the device. The f_t obtained by TCAD simulation is f_t = 220 GHz for $Al_{0.3}Ga_{0.7}N$ HEMT with AlN dielectric for L_g=0.5µm and W=50 µm at V_d=15 V .

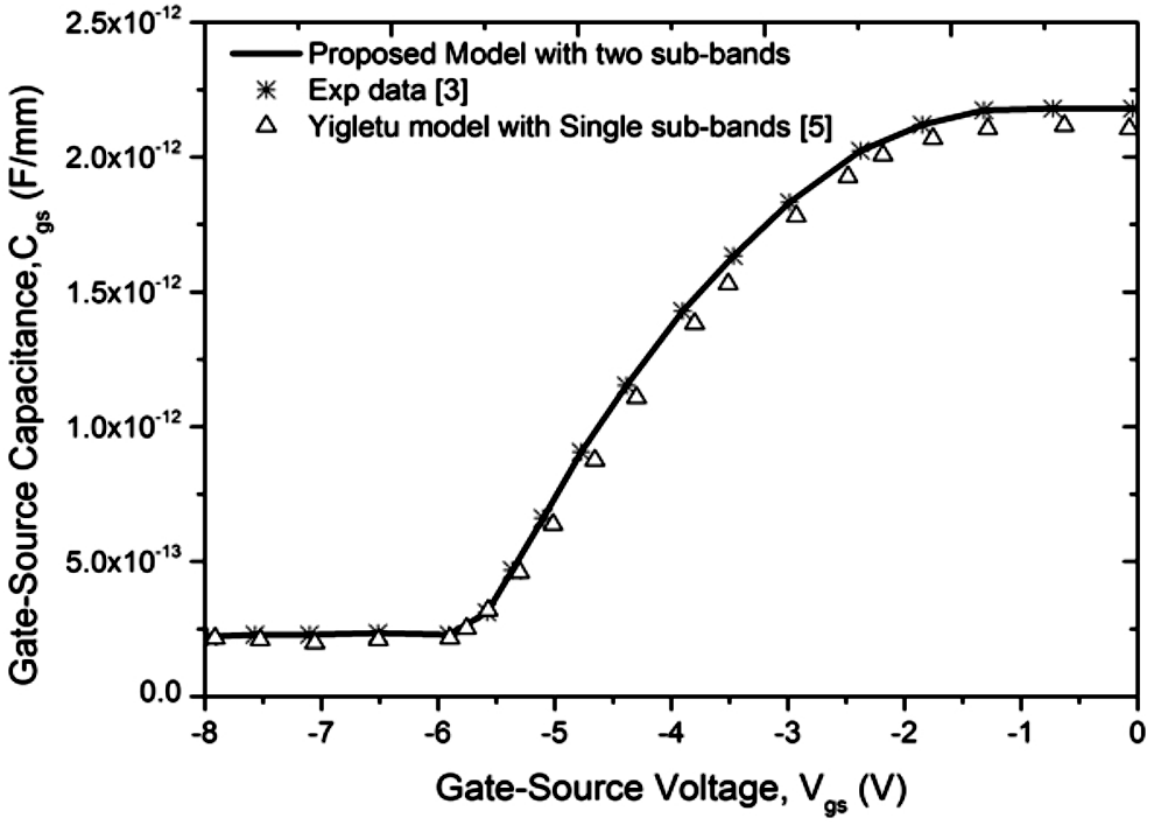

Figure 7: (*a*) Comparison of modeled Gate source capacitance C_{gs} with experimental data for $Al_{0.25}Ga_{0.75}N$/GaN MISHEMT for gate length and width L_g=2.5µm & W=60 µm at a drain voltage of 1V. Experimental data is taken from [3].

6. CONCLUSION

A unique physics-based model for gate charge and capacitances of $Al_xGa_{1-x}N$/AlN/GaN MISHEMT with AlN dielectric have been presented, considering the two lowest subbands (E_0 and E_1) in the triangular well. The proposed model does not have any empirical or fitting parameters, but it shows excellent agreement with experimental data [3,11,12] validating the model.

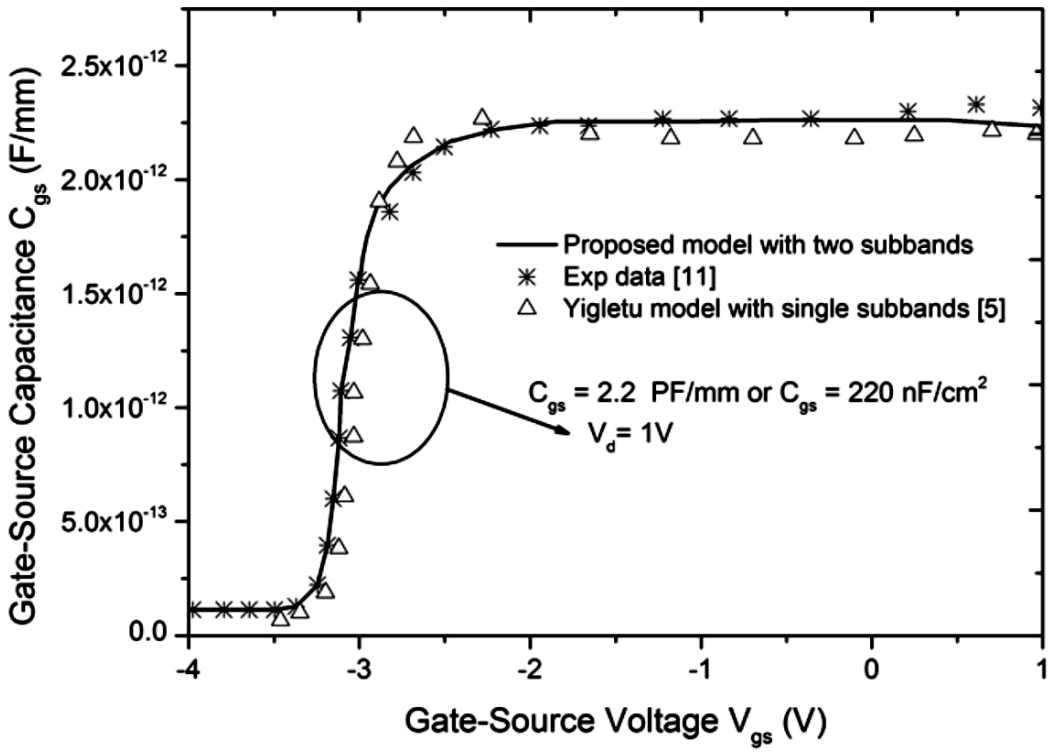

Figure 7: (*b*) Comparison of modeled Gate source capacitance C_{gs} with experimental data for $Al_{0.3}Ga_{0.7}N$/GaN MISHEMT gate length and width L_g=0.5µm, W=50µm. Experimental data is taken from [11]

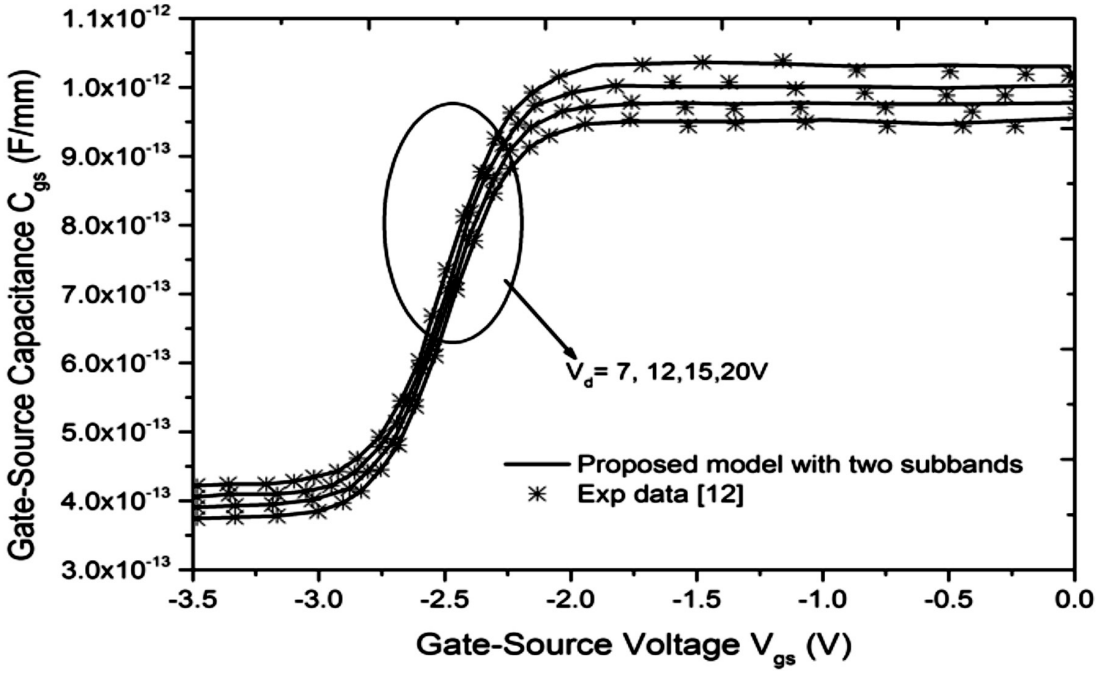

Figure 7: (*c*) Comparison of modeled Gate source capacitance C_{gs} with experimental data for $Al_{0.3}Ga_{0.7}N$/AlN/GaN HEMT for gate length L_g = 0.35µm and W= 25µm. Experimental data is taken from [12] for various drain voltages

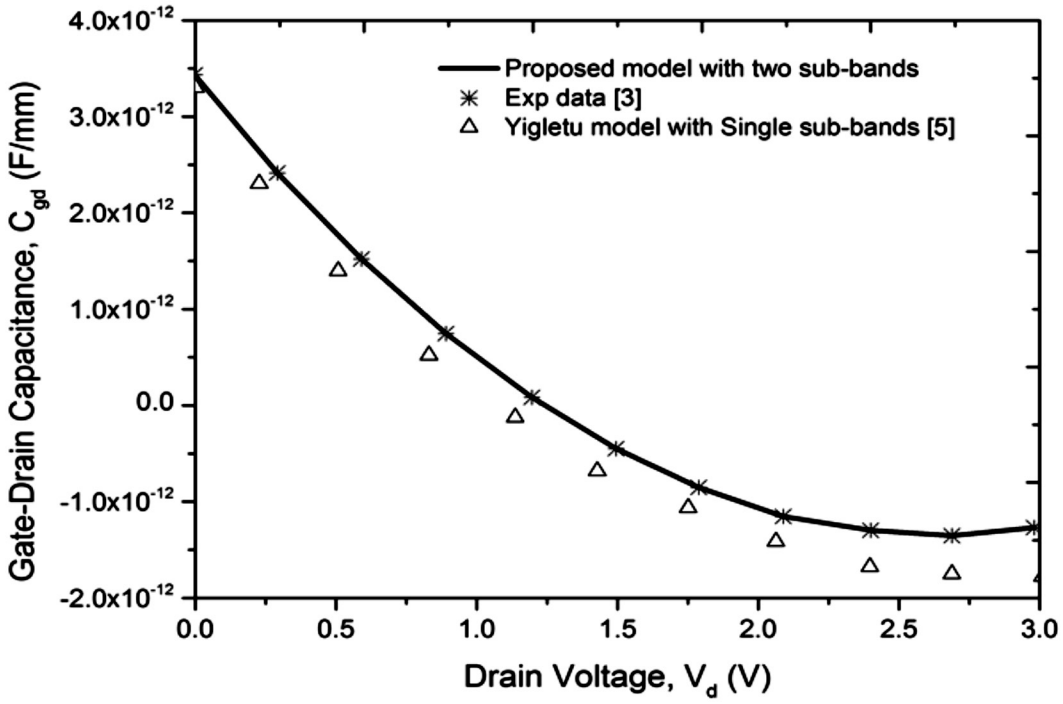

Figure 8: Comparison of Gate drain capacitance, C_{gd} versus drain voltage with experimental data [3], at a gate voltage of -1 V for gate length and width L_g=2.5µm, W=60µm.

Moreover, the effects of sheet carrier density (n_s) on the bias voltages have been comprehensively investigated. The DC current, capacitance C_{gs} and C_{gd} are obtained analytically under different bias voltages including SCEs.

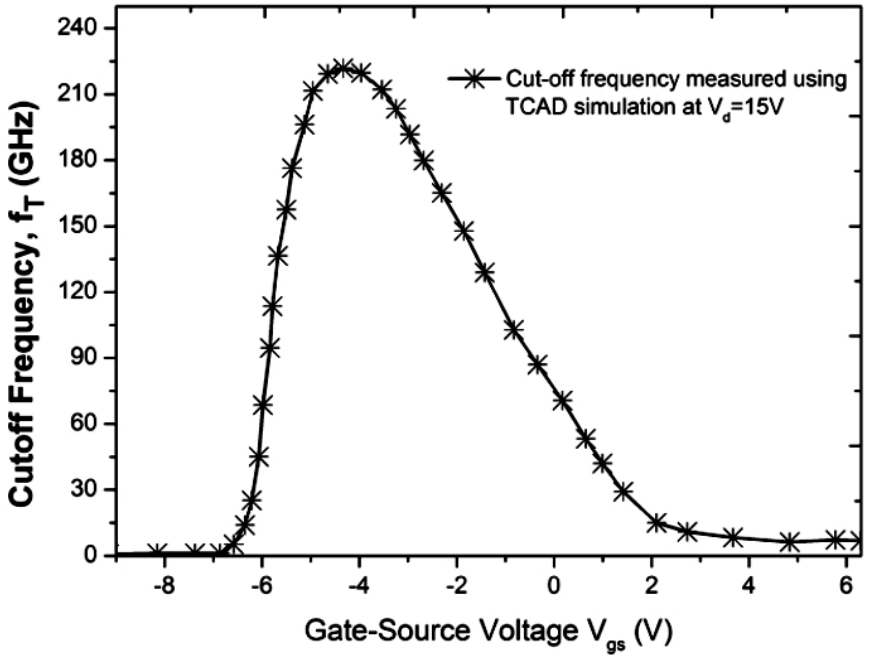

Figure 9: Variation of cutoff frequency, f_t with V_{gs} for gate length and width L_g= 0.5µm, W = 50 µm

Table 1
Model parameters for the measured $Al_xGa_{1-x}N$/AlN/GaN MIS-HEMT with AlN dielectric. Parameters used for calculation of n_s, I_{ds} , capacitance and cutoff frequency.

Parameter	*Exp [3] Sample A*	*Exp[11] Sample B*	*Exp[12] Sample C*
$\gamma_0(V.m^{4/3})$	2.5 x10^{-12}	2.5 x10^{-12}	2.5 x10^{-12}
$\gamma_1(V.m^{4/3})$	3.2 x10^{-12}	3.2 x10^{-12}	3.2 x10^{-12}
n_s (cm^{-2})	9.86×10^{12}	7.2×10^{12}	9.86×10^{13}
t_{cap}	5nm	2nm	0nm
D_w ($m^{-2}.V^{-1}$)	3.24x10^{17}	3.24x10^{17}	3.24x10^{17}
$d_{eff} = d_d + d_i\ (nm)$	24	26	18
L_g(μm)	2.5	0.5	0.7
W(μm)	60	50	25
t_{ins} (nm)	10.6	20	0
V_{off}(V)	-5.7	-3.2	-3.8
v_{sat} (m/s)	1.19x10^5	1.19x10^5	1.19x10^5
λ (v^{-1})	1E-6	1E-6	1E-6
μ_0 (m^2/V s)	0.08	0.08	0.08

The developed model covers all operating regions of the MISHEMTs and match well with experimental data. The role of AlN dielectric with increasing DC and RF performance of the device is explored well and this model is reliable in predicting the device behavior of GaN MISHEMTs based analog, power switching circuits and shows a good promise for RF circuit simulations at high frequencies.

REFERENCES

[1] Junbin Zhang ; B. Syamal ; Xing Zhou ; S. Arulkumaran , 2014, A Compact Model for Generic MIS-HEMTs Based on the Unified 2DEG Density Expression, IEEE Electron Devices Society, Feb. 2014, pp.314 - 323.

[2] Zhiwei Bi, Xian, Yue Hao, Hongxia Liu, Linjie Liu , 2009, Characteristics analysis of gate dielectrics in AlGaN/GaN MIS-HEMT, Electron Devices and Solid-State Circuits, , EDSSC 2009, pp.419 - 422.

[3] Xiao-Yong Liu, Sheng-Xun Zhao, Lin-Qing Zhang, Hong-Fan Huang, Jin-Shan Shi, Chun-Min Zhang, Hong-Liang Lu, Peng-Fei Wang , David Wei Zhang ,2015, AlGaN/GaN MISHEMTs with AlN gate dielectric grown by thermal ALD technique, Nanoscale Research Letters, December 2015, pp. 10:109.

[4] Sourabh Khandelwal, T.A. Fjeldly, 2012, A physics based compact model of I–V and C–V characteristics in AlGaN/GaN HEMT devices , Solid-State Electronics, Volume 76, October 2012, pp. 60–66.

[5] F. M. Yigletu, Tarragona, Spain ; S. Khandelwal ; T. A. Fjeldly ; B. Iñiguez , 2013, Compact Charge-Based Physical Models for Current and Capacitances in AlGaN/GaN HEMTs, IEEE Transactions on Electron Devices , Nov. 2013. (Volume:60 , Issue: 11), pp.3746 - 3752 ,

[6] Wang Jie; Sun Lingling, Liu Jun, and Zhou Mingzhu , 2013, A surface-potential-based model for AlGaN/AlN/GaN HEMT , Journal of Semiconductors, September 2013, Vol. 34, pp. 9.

[7] X. Cheng, M. Li, and Y. Wang, 2009, Physics-based compact model for AlGaN/GaN MODFETs with close-formed I–V and C–V characteristics, IEEE Trans. Electron Devices, Dec 2009, vol. 56, no. 12, pp. 2881–2887.

[8] A. Mohanbabu, N. Anbuselvan, N. Mohankumar, D. Godwinraj, C.K. Sarkar, 2014, Modeling of sheet carrier density and microwave frequency characteristics in Spacer based AlGaN/AlN/GaN HEMT devices, Solid-State Electronics, Volume 91, January 2014, pp. 44–52.

[9] S Baskaran, A Mohanbabu, N Anbuselvan, N Mohankumar, D Godwinraj, CK Sarkar, 2013, Modeling of 2DEG sheet carrier density and DC characteristics in spacer based AlGaN/AlN/GaN HEMT devices, Superlattices and Microstructures, 64 (2013),pp. 470–482.

[10] Chen Tangsheng,Jiao Gang, Li Zhonghui, Li Fuxiao,Shao Kai,Yang Naibin, 2006 AlGaN/AlN/GaN MISHEMT with AlN dielectric, CS MANTEC conference, April 24-27,2006, Vancouver, British Colombia, Canada.

[11] Jie-Jie Zhu, Xiao-Hua Ma,Yong Xie, Bin Hou, Wei-Wei Chen, Jin-Cheng Zhang, and Yue Hao, 2015, Improved Interface and Transport Properties of AlGaN/GaN MIS-HEMTs With PEALD-Grown AlN Gate Dielectric, IEEE Transactions On Electron Devices, February 2015, Vol. 62, NO. 2.

[12] J.W. Lee and K. J.Webb, 2004, A temperature dependent non-linear analytic model for AlGaN-GaN HEMT on SiC, IEEE Trans. Microw. Theory Tech., Jan. 2004. vol. 52, no. 1, pp. 2–9.

[13] P. Kordoš, D. Gregušová, R. Stoklas, K. Čičo, and J. Novák , 2007,Improved transport properties of Al2O3/AlGaN/GaN metal-oxide semiconductor heterostructure field-effect transistor, Appl. Phys. Lett. 90, 123513 (2007); doi: 10.1063/1.2716846.

[14] C. J. Kao, M. C. Chen, C. J. Tun, and G. C. Chi, 2005, Comparison of low-temperature GaN, SiO2, and SiNx as gate insulators on AlGaN/GaN heterostructure field-effect transistors, Journal Of Applied Physics (2005) 98, 064506.

[15] Xing Zhou, Guojun Zhu, Guan Huei See, Karthik Chandrasekaran, Siau Ben Chiah, Khee Yong Lim,2011, Unification of MOS compact models with the unified regional modeling approach, J Comput Electron (2011) 10:121–135.

[16] Donald E. Ward, and Robert w. Dutton, 1978, Charge-Oriented Model for MOS Transistor Capacitances, IEEE Journal Of Solid-State Circuits, OCTOBER 1978,VOL. SC-13, NO. 5.

[17] Ling-Feng Mao, Huan-Sheng Ning, Jin-Yan Wang, The Current Collapse in AlGaN/GaN High- Electron Mobility Transistors Can Originate from the Energy Relaxation of Channel Electrons, PLoS ONE 10(6):e0128438. doi:10.1371/journal.pone.0128438.

[18] Neamen,1992 ,Semiconductor Physics And Devices, Tata McGraw-Hill Education, 1992.

[19] X. Z. Dang, P. M. Asbeck, and E. T. Yu, 1992, Measurement of drift mobility in AlGaN/GaN heterostructure field-effect transistor, Applied Physics Letters, June 1999, Volume 74, Number 21.

[20] Deng W, Huang J, Ma X, Liou JJ, 2015, An explicit surface potential calculation and compact current model for AlGaN/GaN HEMTs, IEEE Electron Device Lett 2015;36(2):pp.108–10.